

Growth of highly conductive Al-rich AlGa_N:Si with low group-III vacancy concentration F

Cite as: AIP Advances **11**, 095119 (2021); <https://doi.org/10.1063/5.0066652>

Submitted: 11 August 2021 . Accepted: 05 September 2021 . Published Online: 22 September 2021

 Abdullah S. Almogbel,  Christian J. Zollner,  Burhan K. Saifaddin, et al.

COLLECTIONS

F This paper was selected as Featured



View Online



Export Citation



CrossMark

ARTICLES YOU MAY BE INTERESTED IN

[Improved epilayer qualities and electrical characteristics for GaInN multiple-quantum-well photovoltaic cells and their operation under artificial sunlight and monochromatic light illuminations](#)

AIP Advances **11**, 095208 (2021); <https://doi.org/10.1063/5.0062346>

[On the Ge shallow-to-deep level transition in Al-rich AlGa_N](#)

Journal of Applied Physics **130**, 055702 (2021); <https://doi.org/10.1063/5.0059037>

[A first-principles understanding of point defects and impurities in GaN](#)

Journal of Applied Physics **129**, 111101 (2021); <https://doi.org/10.1063/5.0041506>



Call For Papers!

AIP Advances

SPECIAL TOPIC: Advances in Low Dimensional and 2D Materials

Growth of highly conductive Al-rich AlGa_N:Si with low group-III vacancy concentration

Cite as: AIP Advances 11, 095119 (2021); doi: 10.1063/5.0066652

Submitted: 11 August 2021 • Accepted: 5 September 2021 •

Published Online: 22 September 2021











View Online



Export Citation



CrossMark

Abdullah S. Almogbel,^{1,2,a)}  Christian J. Zollner,¹  Burhan K. Saifaddin,²  Michael Iza,¹ Jianfeng Wang,¹ Yifan Yao,¹ Michael Wang,¹ Humberto Foronda,¹  Igor Prozheev,³  Filip Tuomisto,^{3,4}  Abdulrahman Albadri,² Shuji Nakamura,^{1,5}  Steven P. DenBaars,^{1,5}  and James S. Speck¹

AFFILIATIONS

¹Materials Department, University of California, Santa Barbara, California 93106, USA

²King Abdulaziz City for Science and Technology, Riyadh 11442, Saudi Arabia

³Department of Physics and Helsinki Institute of Physics, University of Helsinki, 00014 Helsinki, Finland

⁴Department of Applied Physics, Aalto University, 02150 Espoo, Finland

⁵Department of Electrical and Computer Engineering, University of California, Santa Barbara, California 93106, USA

^{a)}Author to whom correspondence should be addressed: almogbel@ucsb.edu and asalmogbel@kacst.edu.sa

ABSTRACT

The impact of AlGa_N growth conditions on AlGa_N:Si resistivity and surface morphology has been investigated using metalorganic chemical vapor deposition. Growth parameters including growth temperature, growth rate, and trimethylindium (TMI) flow have been systematically studied to minimize the resistivity of AlGa_N:Si. We observed a strong anticorrelation between AlGa_N:Si conductivity and growth temperature, suggesting increased silicon donor compensation at elevated temperatures. Secondary ion mass spectrometry and positron annihilation spectroscopy ruled out compensation by common impurities or group-III monovacancies as a reason for the observed phenomenon, in contrast to theoretical predictions. The underlying reason for AlGa_N:Si resistivity dependence on growth temperature is discussed based on the possibility of silicon acting as a DX center in Al_{0.65}Ga_{0.35}N at high growth temperatures. We also show remarkable enhancement of AlGa_N:Si conductivity by introducing TMI flow during growth. A minimum resistivity of 7.5 mΩ cm was obtained for *n*-type Al_{0.65}Ga_{0.35}N, which is among the lowest reported resistivity for this composition.

© 2021 Author(s). All article content, except where otherwise noted, is licensed under a Creative Commons Attribution (CC BY) license (<http://creativecommons.org/licenses/by/4.0/>). <https://doi.org/10.1063/5.0066652>

I. INTRODUCTION

Al_xGa_{1-x}N (AlGa_N) is a direct ultrawide-bandgap semiconductor that is attracting significant interest for photonics and electronics applications; AlGa_N has several favorable features that include large direct bandgap, high electric breakdown field, and low intrinsic carrier concentration,^{1,2} which will enable high voltage, high frequency, and low noise operation for next-generation switching electronics.^{3,4} With its tunable bandgap property, Al-rich AlGa_N enabled the development of deep UV LEDs and lasers for water and air purification.⁵⁻⁸ It also enabled the development of high power electronics and transistors that can be employed in a wide variety of applications such as smart grids, electric vehicles, and solar cell inverters.⁹ Other potential applications of AlGa_N include chemical sensing,¹⁰ atomic clocks and sensors,¹¹ solar-blind free-space optical communications,¹² and solar-blind UV photodetectors.¹³

Achieving low-resistivity AlGa_N is essential to fabricate high performance devices, primarily by minimizing the voltage losses and ohmic heating, which can lead to material degradation and premature failure.^{14,15} Al_{0.65}Ga_{0.35}N is of special interest in the heterostructure design of UVC emitters because it is optically transparent and when employed as a quantum barrier, it forms a sufficient conduction band offset to create strong electron confinement and minimize leakage current.¹⁶ Undoped AlGa_N with high aluminum content can exhibit resistivity as high as 10⁵ Ω cm.¹⁷ Silicon (Si) is the standard *n*-type dopant for III-N materials, acts as a substitutional donor in the group-III sites, and donates one electron (Si_{III})⁺.¹⁸ In Al-rich AlGa_N, Si has shallower donor activation energy than other candidate donors such as germanium on cation sites¹⁹ or sulfur and oxygen on the anion sites.²⁰

Theoretically, Si is expected to be incorporated as a shallow donor in AlGa_N up to 94% Al mole fraction,²¹ which has been

experimentally confirmed up to 84% Al mole fraction.²² Above a certain critical composition, the *DX* configuration for Si becomes more energetically favorable, and the donor ionization efficiency drops rapidly.^{23,24} In addition, with increasing Al content in AlGa_xN, compensation of the Si donors by the formation of group-III vacancies, which act as deep acceptors, becomes more favorable.²⁵

Several groups have achieved low-resistivity Al_xGa_{1-x}N:Si with $\rho < 10 \text{ m}\Omega \text{ cm}$ for Al content $x > 0.6$ by metalorganic chemical vapor deposition (MOCVD), often by optimizing the silicon/III molar ratio,^{26–29} or by growing on a substrate with low defect density.^{30–33} In this work, we show that the AlGa_xN growth temperature strongly impacts the AlGa_xN:Si conductivity and in some cases has a stronger effect than silicon precursor flow. We investigated the mechanism of silicon donor compensation in AlGa_xN:Si by secondary ion mass spectrometry (SIMS) and positron annihilation spectroscopy (PAS). Our results ruled out the possibility of silicon donor compensation by common impurities or group-III monovacancies. Moreover, we investigated the impact of trimethylindium (TMI) flow and growth rate (GR) on AlGa_xN:Si resistivity and morphology and discovered that the TMI flow, with no detectable In incorporation into the epitaxial layers, decreases the resistivity of AlGa_xN:Si by a factor of two.

II. EXPERIMENTS

The films were grown on nominally vicinal Si-face *c*-plane 6H-silicon carbide (SiC) substrates using low-pressure horizontal MOCVD (TNSC SR4000-HT). There are two main advantages for growing AlGa_xN on SiC substrates in contrast to sapphire substrates. First, SiC has a similar crystal structure to wurtzite AlGa_xN with small lattice and thermal mismatch, and thus, AlN growth on SiC is believed to generate fewer threading dislocations than sapphire, as we have recently shown.³⁴ Another advantage of SiC for UV application is that it is easily compatible with thin-film flip-chip processing and can be used to develop high-light extraction UV LEDs.^{35–37} For AlGa_xN growth, the reactor pressure was fixed at 150 Torr to increase the effective surface mobility of aluminum adatoms. The precursors for aluminum, gallium, and indium were trimethylaluminum (TMA), trimethylgallium (TMG), and trimethylindium (TMI), respectively. Diluted Si₂H₆ (10%) in H₂ gas was the silicon precursor, and ammonia (NH₃) gas, the nitrogen source. Prior to growth, the SiC was treated *in situ* with NH₃/H₂ at $T > 1250 \text{ }^\circ\text{C}$, which we have found prevents cracking^{34,38} (all samples in this work were crack-free as confirmed by optical microscopy). Growth temperatures were measured with a thermocouple located in an opening in the heater assembly. Planar AlN layers were grown as a template with an estimated threading dislocation density of around $10^9/\text{cm}^2$, the details of which were described elsewhere.³⁹ A 200 nm-thick undoped Al_{0.8}Ga_{0.2}N buffer was then grown on the 1 μm -thick AlN template layer, followed by 500 nm-thick silicon-doped Al_xGa_{1-x}N, where x was calibrated to 0.65. The NH₃ flow was fixed at 2 Standard Litre per Minute (SLM) during AlGa_xN growth.

The composition and relaxation of the AlGa_xN:Si layers were evaluated by the analysis of the AlGa_xN and AlN peak separation using reciprocal space mapping (RSM) via the (10 $\bar{1}$ 5) reflection (*hkil* notation) measured in an asymmetric scattering geometry. The underlying AlN layer was confirmed to be fully relaxed.³⁴ We applied Vegard's law for the AlGa_xN lattice and elastic constants.

RSMs were recorded using a high-resolution XRD system equipped with a monochromatic Cu-K α_1 source and a 2D array detector. The evaluated composition was cross-correlated with cathodoluminescence (CL) peak measurements of the AlGa_xN emission wavelength to minimize the composition error. Atom probe tomography confirmed the random alloy distribution of AlGa_xN and that no clusters of Ga or Al were observed.⁴⁰

Dynamic SIMS with a magnetic-sector mass filter was used to quantify the elemental concentration of AlGa_xN dopants. Cesium was used as a source for the highly focused primary ion beam to maximize the ionization yield of the AlGa_xN surface. The primary Cs⁺ ion beam energy was fixed at 15 kV, and silicon concentration measurements were performed using high mass resolving power to distinguish between the mass spectral peaks of ²⁸Si, N₂, and ²⁷Al ¹H complexes that are narrowly spaced in the mass spectrum. Surface imaging and roughness statistics of the AlGa_xN:Si surface were determined by atomic force microscopy (AFM) in a non-contact tapping mode. Hall-effect measurements were carried out at room-temperature (RT) under varying magnetic field **B** normal to the sample surface, swept from -0.6 to $+0.6 \text{ T}$ to measure the resistivity (ρ), electron concentration (n), and mobility (μ) of the AlGa_xN:Si layer. Hall measurements were carried out using the van der Pauw configuration. The measurement pattern was formed on the AlGa_xN:Si surface using standard photolithography and plasma etching, and then the metal stack of V (20 nm)/Al (100 nm)/V (100 nm)/Au (200 nm) annealed at 740 $^\circ\text{C}$ in N₂ for 30 s was used for n-ohmic contact metal. The underlying layers (i.e., Al_{0.8}Ga_{0.2}N/AlN) insulated the AlGa_xN:Si from SiC as confirmed by electrical measurements.

Positron annihilation spectroscopy (PAS) experiments in the Doppler broadening mode were conducted with a slow positron beam at 10 keV to estimate the concentrations of negative and neutral cation vacancies (V_{III} and V_{III}-related complexes) in the AlGa_xN:Si layers. High purity germanium detectors with a resolution of 1.25 keV at the 511 keV annihilation line were employed to collect $\sim 10^6$ counts in the annihilation spectra. The *S* parameter was defined as the fraction of counts around the $<0.96 \text{ keV}$ -wide central region of the peak, and the *W* parameter is the fraction of counts in the tail of the peak at the energy range of $\pm(3.00\text{--}7.60 \text{ keV})$ from the center. Details of the experimental approach and analyses can be found elsewhere.^{41,42}

III. RESULTS AND DISCUSSION

A. AlGa_xN growth calibration

Growth of UVC LEDs requires various AlGa_xN compositions. For instance, the active region consists of Al_{0.40}Ga_{0.60}N quantum wells, Al_{0.65}Ga_{0.35}N quantum barriers, and an Al_{0.80}Ga_{0.20}N electron blocking layer. Hence, it is imperative to map out the AlGa_xN growth space and study the composition/wavelength relationship. Therefore, both RSM and CL were used to analyze the AlGa_xN composition and bandgap. Figure 1(a) shows the cross-correlation between RSM and CL data. These data points were then fit using quadratic regression analysis to model a quadratic bandgap formula $E_g^{\text{AlGa}_x\text{N}}(x) = (1-x)E_g^{\text{Ga}_x\text{N}} + xE_g^{\text{AlN}} - b_{\text{eff}}x(1-x)$, which is commonly used for ternary alloys,⁴³ where x denotes the AlN molar fraction of AlGa_xN. The effective bowing parameter b_{eff} can then be computed using the

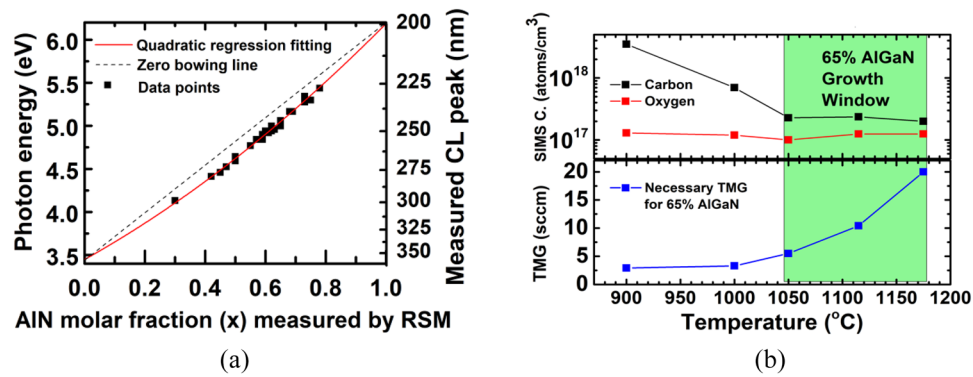


FIG. 1. (a) The Al molar fraction in wurtzite AlGaN was determined by analysis of x-ray diffraction reciprocal space mapping (which considers both a and c lattice parameters to decouple the alloy fraction and strain), and cathodoluminescence was used to determine the energy of the band-edge luminescence. Good agreement is shown with an expected quadratic relation (line fit) between band-edge luminescence and the alloy fraction inferred from the lattice constant using linear Vegard's law. (b) Dependence of impurity incorporation and necessary TMG flow on growth temperature of $\text{Al}_{0.65}\text{Ga}_{0.35}\text{N}$. At elevated growth temperatures, higher TMG flow was necessary to grow a particular AlGaN composition, indicating a higher desorption rate of gallium adatoms as the growth temperature increases. TMA flow was fixed to 10 SCCM (equivalent to $\text{GR} = 1 \text{ \AA/s}$).

bandgap values of E_g^{GaN} and E_g^{AlN} at RT. We determined the bowing parameter of our AlGaN material to be $b_{\text{eff}} = +0.8 \pm 0.2 \text{ eV}$ as derived from the quadratic regression fitting formula assuming $E_g^{\text{AlN}} = 6.2 \text{ eV}$ and $E_g^{\text{GaN}} = 3.44 \text{ eV}$ at 300 K. Uncertainty in b_{eff} is partially due to the lack of consensus on the exact bandgap of AlN at 300 K.⁴⁴ The reported AlGaN bowing parameter varies widely in the literature from -0.8 to $+2.6 \text{ eV}$,⁴³ but a value of $+0.7 \text{ eV}$ is generally recommended.⁴⁵ The positive curvature of AlGaN bowing is shown in Fig. 1(a).

Figure 1(b) summarizes AlGaN growths at temperatures between 900 and 1175 °C, showing the necessary TMG flow required to target 65% AlGaN while keeping the TMA fixed at a 10 SCCM flow. It was found that the TMG flow necessary to sustain 65% Al content AlGaN had exponential dependence on temperature, which is consistent with gallium desorption-limited growth.⁴⁶ The Arrhenius plot fit yields an activation energy of $E_A = 28 \text{ kcal/mol}$ ($=1.23 \text{ eV/atom}$) for Ga desorption from the AlGaN surface, which is higher than E_A of Ga desorption from the GaN surface under the same growth conditions.⁴⁷ We observed that, under this particular growth regime, the AlGaN GR was limited by the TMA flow rate whereas the composition was controlled by TMG flow. For temperatures $>1200 \text{ °C}$, the Ga desorption rate significantly exceeds the Ga incorporation rate, and the AlGaN composition cannot be reliably maintained by the TMG flow rate, setting a practical upper limit on the growth temperature range of AlGaN.

The dependence of the unintentional carbon and oxygen impurity incorporation on growth temperature shows that temperatures $>1050 \text{ °C}$ yielded the lowest concentrations [Fig. 1(b)]. It was expected that carbon incorporation would decrease as the growth temperature increased due to the decomposition of carbon-containing reaction by-products at higher temperatures. The oxygen impurity concentration was insensitive to the growth temperature in the range 900–1175 °C, which may be attributed to the low water vapor content in the precursors, chamber, and carrier gas.⁴⁸

B. Temperature effect

Several growth experiments were conducted to study the effect of growth parameters (i.e., T , GR, and TMI flow) on the conductivity of AlGaN:Si. Figure 2 summarizes the key results of these experiments and compares the resistivity of AlGaN:Si layers grown under various growth temperatures of 1175, 1115, and 1050 °C—all within the identified low-impurity growth window [see

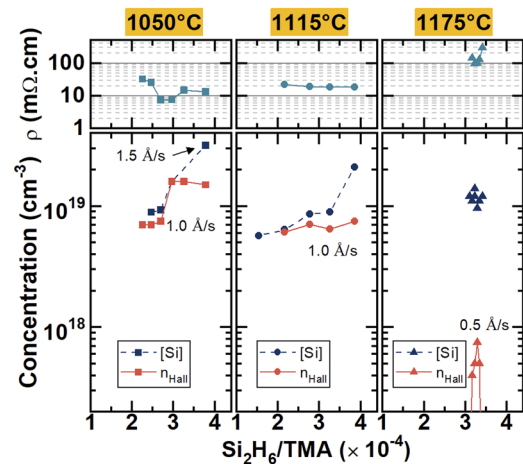


FIG. 2. The dependence of the electron concentration determined by Hall measurements on disilane/TMA molar ratio for various growth conditions: fast growth at 1050 °C, fast growth at 1115 °C, and slow growth at 1175 °C. AlGaN:Si grown at lower temperatures had a wider optimal doping window, higher n , and lower resistivities, while AlGaN:Si grown at higher temperature had a narrower optimal doping window and experienced an earlier onset of overdoping behavior. In all growth modes, the free electron concentration n peaked at approximately the same optimal disilane/TMA molar ratio, and n was found to saturate at some temperature-dependent limit even when the silicon concentration increased.

Fig. 1(b)]—maintaining the AlGa_N:Si composition at $65\% \pm 3\%$. The AlGa_N:Si films exhibited high resistivity, a narrow optimal doping window, and limited electron concentration when grown at a high temperature of $T = 1175\text{ }^{\circ}\text{C}$ even with $[\text{Si}] \sim 10^{19}/\text{cm}^3$, showing that high growth temperatures are unfavorable for efficient Si doping. Further experiments (not shown) confirmed that the doping window at $T = 1175\text{ }^{\circ}\text{C}$ remained narrow regardless of the GR or TMI flow. The resistivity decreased and the optimal doping window extended upon reducing the growth temperature to $1115\text{ }^{\circ}\text{C}$, as shown in Fig. 2.

The disilane flow was found to have a weaker influence on the AlGa_N conductivity at lower growth temperatures. At $1175\text{ }^{\circ}\text{C}$, optimization of silicon doping reduced the resistivity from >300 to $87\text{ m}\Omega\text{ cm}$, while at lower temperatures, a wider variation in disilane flow did not result in an abrupt change in resistivity. A further decrease in growth temperature from 1115 to $1050\text{ }^{\circ}\text{C}$ reduced the minimum resistivity from 18.5 to $7.5\text{ m}\Omega\text{ cm}$. In addition, the decrease in growth temperature correlates with the increase in the maximum electron concentration n . For example, n doubled from $7.5 \times 10^{18}/\text{cm}^3$ to $1.6 \times 10^{19}/\text{cm}^3$ upon reducing T from 1115 to $1050\text{ }^{\circ}\text{C}$ for the same $[\text{Si}]$ of $1.5\text{--}2 \times 10^{19}/\text{cm}^3$ as confirmed by SIMS, which shows higher doping efficiency at lower growth temperatures. A further increase in the Si concentration did not result in higher n , as shown in Fig. 2, which suggests that n saturates at a certain growth-temperature-dependent limit.

Growing AlGa_N:Si at reduced temperatures may increase the roughness of the AlGa_N surface, which is typically undesirable in LEDs and lasers. However, AFM micrographs of the surface did not show a marked change in surface morphology with decreasing growth temperature as shown in Fig. 3. For AlGa_N:Si, surfaces appear to have pyramidal hillocks with an average density of $2 \times 10^8/\text{cm}^2$, attributed to the antisurfactant nature of silicon dopants⁴⁹ as the undoped AlGa_N exhibited an atomically flat surface with a well-defined step-terrace structure [Fig. 3(a)]. These growth conditions were optimized with respect to conductivity, not morphology; LED experiments (not shown) demonstrate that the slightly roughened surface can be buried by a smoothing layer. By growing a

15 nm -thick undoped AlGa_N layer at a high growth temperature of $T = 1175\text{ }^{\circ}\text{C}$ on top of the rough AlGa_N:Si layer, atomically flat active region layers can be realized. In the LED experiments (not shown), reducing the AlGa_N:Si growth temperature from 1175 to $1050\text{ }^{\circ}\text{C}$ improved the LED forward voltage without diminishing the MQW optical emission. Overall, we did not observe a noticeable change in the MQW crystal quality or surface morphology upon reducing the AlGa_N:Si growth temperature from 1175 to $1050\text{ }^{\circ}\text{C}$.

SIMS of optimized AlGa_N:Si samples grown at different temperatures showed that the $[\text{Si}]$ is approximately the same in these samples and that $[\text{H}]$, $[\text{O}]$, $[\text{C}]$, and $[\text{Mg}]$ were all in the range of $10^{16}\text{--}10^{17}/\text{cm}^3$, as shown in Fig. 4(a)—insufficient to account for the increased compensation of Si.

C. Positron annihilation measurements

Since the Ga desorption rate is higher at $1175\text{ }^{\circ}\text{C}$ than at $1050\text{ }^{\circ}\text{C}$, we considered the possibility of compensation by group-III triple acceptor monovacancies V_{III}^{3-} , as well as compensation by $V_{\text{III}}\text{--H}$ complexes, which may act as double acceptors $(V_{\text{III}}\text{--H})^{2-}$ or single acceptors $(V_{\text{III}}\text{--H}_2)^{1-}$ in n -type III-nitrides.^{50–52} Positron annihilation spectroscopy (PAS) was carried out on six samples, with two samples with different silicon flows for each growth temperature, to examine the hypothesis of compensation by V_{III} . Figure 4(b) shows relative S and W annihilation parameters measured in the Si-doped AlGa_N alloys. The (S, W) parameters are shown normalized to the MBE-grown Mg-doped GaN reference that is known to produce the annihilation characteristics of the GaN lattice. Characteristic points representing the GaN lattice, AlN lattice, V_{Al} in AlN, and typical grown-in Ga vacancies in GaN (denoted by $V_{\text{Ga}}\text{--X}$) are also shown.^{53–55} The (S, W) data points of five out of six samples lie very close to the line connecting GaN and AlN, which means that in these samples, the V_{III} -related vacancy defect concentration is at the RT detection limit of $\text{low-}10^{16}/\text{cm}^3$. For the sample grown at $1115\text{ }^{\circ}\text{C}$ with $n = 6.5 \times 10^{18}/\text{cm}^3$, the (S, W) data points are shifted toward the vacancy-characterizing points, and the distance from the GaN-AlN line allows us to estimate the V_{III} concentration in these

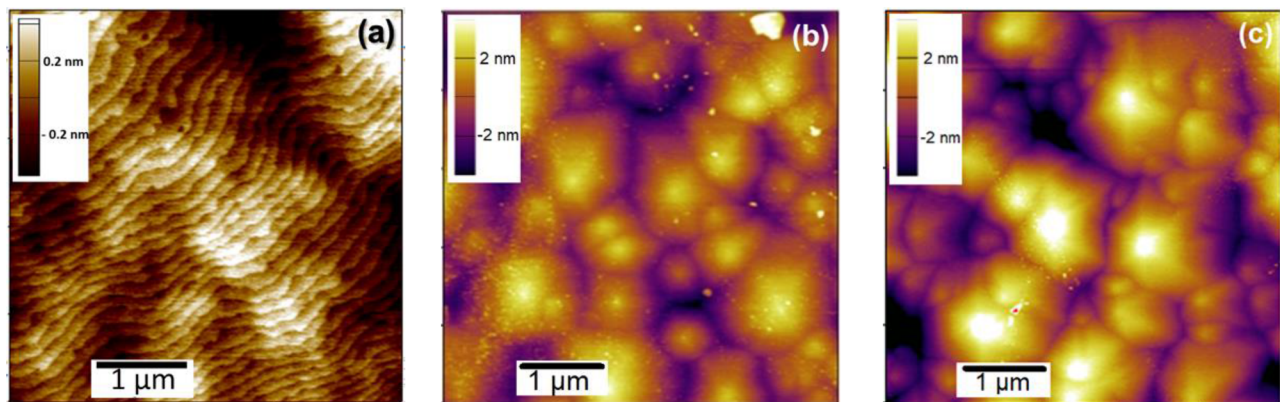


FIG. 3. AFM images of AlGa_N:Si layers (optimized with respect to resistivity) grown at different temperatures. (a) Undoped AlGa_N. (b) AlGa_N:Si grown at $T = 1050\text{ }^{\circ}\text{C}$ ($\text{RMS} = 1.4\text{ nm}$). (c) AlGa_N:Si grown at $T = 1175\text{ }^{\circ}\text{C}$ ($\text{RMS} = 1.9\text{ nm}$). These films were grown at $1\text{ }^{\text{Å}}/\text{s}$, and samples grown at a slower growth rate of $0.5\text{ }^{\text{Å}}/\text{s}$ exhibited similar hillock-mediated surface morphology with comparable smoothness, likely indicating that the silicon-induced roughening is controlling the AlGa_N:Si surface quality more than the growth temperature or growth rate in this growth regime.

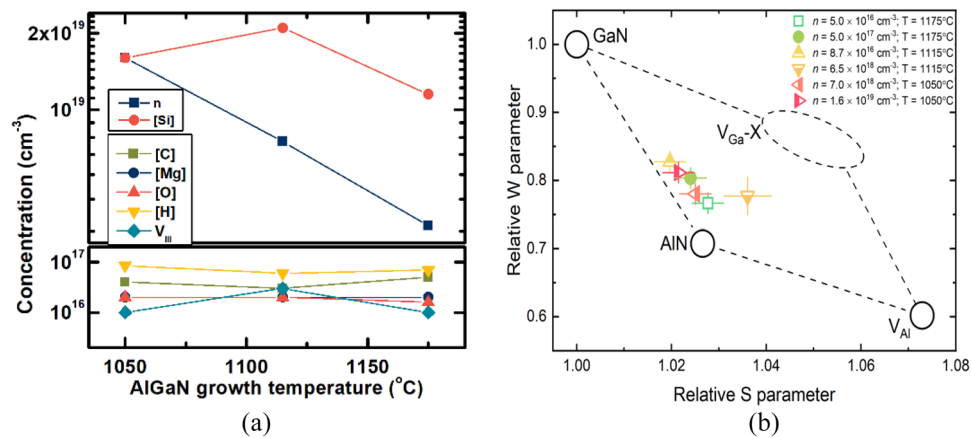


FIG. 4. (a) Comparison of silicon, carbon, magnesium, oxygen, and hydrogen concentration from SIMS as well as electron concentration from Hall measurements and group-III monovacancy estimates from PAS. No atomic impurities can explain donor compensation behavior. All films were grown at TMA = 10 SCCM. All SIMS measurements were calibrated using relative sensitivity factors from ion-implanted AlGa standards and have relative uncertainties of ~20%. (b) Relative S and W parameters measured in AlGa:Si samples. Parameters characterizing the GaN lattice, AlN lattice, and isolated V_{Al} in AlN are marked with big open circles. The dashed oval marks the region of the (S, W) parameters for in-grown V_{Ga} complexed with H, O, or N impurities in GaN. Samples at 1050 and 1115 °C are grown with TMI surfactant flow, and samples grown at 1175 °C are without TMI surfactant flow, but no significant change in $[V_{III}]$ was observed.

samples to be in the mid- $10^{16}/\text{cm}^3$. No trend is observed in $[V_{III}]$ either with AlGa growth temperature or with Si doping. The independence of the V_{III} concentration of Si doping is in contrast to what was observed by Uedono *et al.*⁵⁶ in 60% AlGa:Si, but in that work, the overall vacancy concentrations were found to be low. Generally, from the point of view of electrical compensation, Si doping has not been found to induce significant V_{III} concentration either in GaN^{53,57} or in AlGa up to 60%–65% of Al content.^{56,58–61}

Importantly, the PAS data show that group-III vacancy concentration is insufficient in our Si-doped 65% AlGa to compensate the Si donors and account for the change in resistivity with growth temperature. It is possible that the acceptor-like impurities (Mg, C, and H), with an overall concentration of the order of $10^{17}/\text{cm}^3$, act as negative ions that are known to be efficient positron traps even at RT in AlN and hence also possible in Al-rich AlGa. If this is the case, our estimated vacancy concentrations would be too low by a factor of 2–3,^{41,54} but the actual concentrations would be still too low for being important for electrical compensation. Another possibility could be the emergence of high concentrations of negatively charged nitrogen vacancies (V_N) that would also act as negative ions in the positron data, reduce the apparent V_{III} concentration, and compensate the donors,^{62–65} but this appears unlikely as the V_N formation energies are higher than those of V_{III} in both n -type GaN and AlN (in N-rich conditions).^{25,66} Of the common native defects (vacancies, interstitials, antisites, ...), the group-III monovacancies are predicted to have the lowest formation energy in Al-rich AlGa:Si and AlN:Si,^{18,25,67–69} yet they were not found in sizable concentration by PAS in our films. Therefore, it is reasonable to assume that defects with higher formation energies such as antisites, vacancy complexes, and interstitials will typically incorporate in lower concentrations than group-III monovacancies.^{70,71}

In a PAS study by Chichibu *et al.*,⁶⁰ a positive correlation was observed between $[V_{III}]$ and $[Si]$, and hence, (V_{III} -nSi) complexes were suggested as possible compensators. However, this possibility

appears unlikely in our materials, given the absence of correlation between $[V_{III}]$ with T or $[Si]$ in our measurements, and the high formation energy of these complexes compared to V_{III} .^{24,69} PAS confirmed the low concentration of negative and neutral (V_{III} -nSi) complexes in our materials, $<10^{17}/\text{cm}^3$. Likewise, complexes of V_{III} with impurities such as (V_{III} -O and V_{III} -C) are expected to be lower than $10^{17}/\text{cm}^3$, given the low concentration of [O] and [C] as confirmed by SIMS [Fig. 4(a)]. We note that PAS is sensitive to both negative and neutral vacancy-type defects, as explained in detail by Tuomisto and Makkonen.⁴¹ At room temperature, the difference in PAS sensitivity to negative and neutral vacancy-type defects is of the order of a factor of 2.⁴¹

D. SIMS and PAS analysis

Figure 4(a) summarizes the key findings of this study: it compares the Hall measurements of n with PAS measurements of $[V_{III}]$, as well as SIMS concentrations of Si and other impurities (C, H, O, and Mg). In high Al content AlGa, impurities such as C, H, and Mg act as acceptors whereas O acts as a deep donor and therefore may compensate the Si donors. Nonetheless, at $T = 1050^\circ\text{C}$, Si donors exhibit limited compensation at $[Si] = 1.6 \pm 0.5 \times 10^{19}/\text{cm}^3$ ($n = 1.6 \times 10^{19}/\text{cm}^3$ from Hall measurements). However, as the growth temperature increases, n decreases despite no significant change in $[Si]$, impurity uptake, or group-III monovacancies—a behavior that is consistent with the possibility of Si undergoing a DX transition.

Several theoretical studies have predicted that silicon in high Al content AlGa can displace from the substitutional site toward an interstitial site and thus form a DX center (shallow donor to deep acceptor transition).^{18,21,25,67} Hydrostatic pressure (HP) studies using diamond anvil cells have experimentally confirmed the emergence of localized DX centers in III-nitrides and shown that they are stable in a compressed crystal lattice. Particularly, in

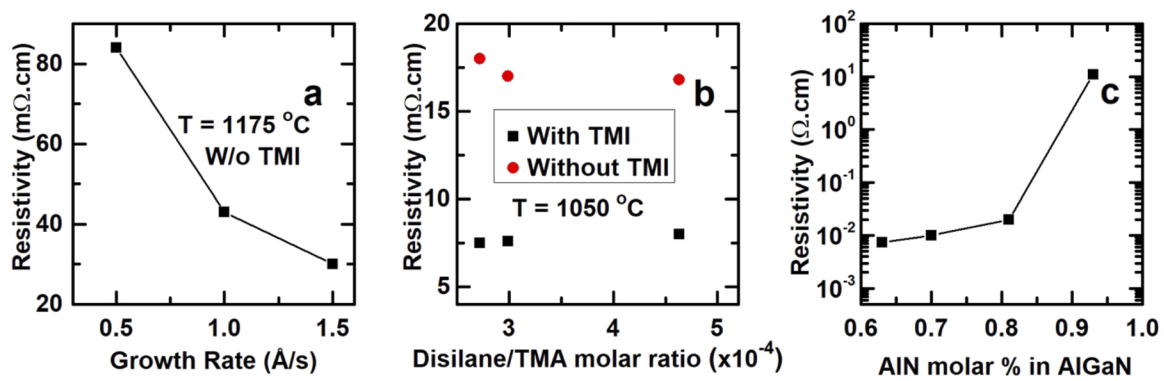


FIG. 5. (a) Resistivity of 65% AlGaIn:Si grown at $T = 1175$ °C (without TMI flow) decreases monotonically with an increasing GR. TMI flow did not result in resistivity reduction at $T = 1175$ °C. (b) TMI impact on 65% AlGaIn:Si resistivity grown at $T = 1050$ °C and $GR = 1$ Å/s showing a decrease in resistivity by a factor of 2 even though no indium incorporation was detected by SIMS and no significant impact on $[V_{III}]$ estimated by PAS. The increase in GR at $T = 1050$ °C did not further improve the resistivity below 7.5 mΩ cm. (c) AlGaIn:Si resistivity as a function of AlN molar fraction in the range 0.6–0.9. The AlGaIn remains highly conductive up to 80%. The abrupt increase in resistivity as x exceeds 0.8 has been widely reported. All films were grown with TMI at $GR = 1$ Å/s.

n-GaIn under both dilute and degenerate doping conditions, it was demonstrated by Wetzel *et al.*⁷² that a critical HP of $p = 20$ GPa depopulated the conduction band of free electrons and caused carrier freezeout. Calculations suggest that the effect of compressive HP on DX formation in *n*-GaIn is equivalent to the effect of alloying with AlN.⁷³ Accordingly, Wetzel *et al.* estimated that GaIn:Si under $p = 25$ GPa is equivalent to Al_{0.56}Ga_{0.44}In in this respect. Skierbiszewski *et al.* confirmed by HP the coexistence of shallow Si donors and localized DX centers in Al_{*x*}Ga_{1-*x*}In at RT up to $x = 0.6$ ⁷⁴ and measured the impact on resistivity under much lower applied pressure than *n*-GaIn, which may be indicative of shallower formation energy threshold.²²

Overall, we found that (1) the incorporation of impurities and monovacancies was at least two orders of magnitude lower than the silicon concentration, (2) there was no large variation in silicon concentration among optimized AlGaIn:Si samples grown at different temperatures, (3) the free electron concentration decreased with increasing growth temperature, and (4) low-resistivity AlGaIn:Si with higher aluminum composition was grown at lower temperatures for the same optimal disilane/Al ratio [Fig. 5(c)]. Therefore, we tentatively attribute the compensation in our heavily silicon-doped AlGaIn to the formation of DX centers. However, we cannot discount the role of impurities that we have not measured in SIMS or nitrogen vacancies V_N in the overall behavior. We note that in AlN, V_N are predicted to be acceptors for Fermi levels near the conduction band (e.g., see Fig. 2 in Ref. 25). In addition, we note that Si DX in AlGaIn is not only a function of the average Al composition but also depends on the Si doping level and Al atomic coordination around the Si donor as shown by Mooney *et al.*⁷⁵

E. Effect of GR and TMI flow

The effect of the GR on the properties of the AlGaIn:Si layers was also investigated and found to impact the AlGaIn:Si resistivity but only at higher growth temperatures. The GR was varied between 0.5 to 1.5 Å/s. The increase in GR at $T = 1175$ °C reduced the resistivity from 87 to 30 mΩ cm as shown in Fig. 5(a). The GR increase

was affected by increasing the TMA flow, keeping the disilane/TMA ratio, TMG, and NH₃ flows unchanged. The AlGaIn composition did not vary by increasing the TMA flow, and the AlGaIn:Si films remained smooth at both $T = 1175$ and $T = 1050$ °C as shown in Fig. 3. In general, smoother films were realized at higher temperatures and slower GRs, as expected from the literature. Deviations from this trend are attributed to differing silicon flow conditions for different growth conditions. Unlike with $T = 1175$ °C, increasing the GR at $T = 1050$ °C did not show further improvement in resistivity below 7.5 mΩ cm [the minimum obtained resistivity as shown in Fig. 5(b)]. We limited the growth rate increase to 1.5 Å/s because the carbon impurity uptake tends to scale with the GR—the higher the GR, the higher the carbon uptake and vice versa.⁴⁸

To investigate the effect of TMI flow on AlGaIn:Si conductivity,⁷⁶ we compared 65% AlGaIn:Si samples with and without 200 SCCM of TMI flow during growth at $T = 1050$ °C. Under different silicon doping conditions, the resistivity decreased by almost half with TMI flow as shown in Fig. 5(b), which is similar to the resistivity improvement obtained in indium-doped GaIn:Mg with $[In] > 10^{19}/\text{cm}^3$.⁷⁷ However, indium incorporation in the AlGaIn:Si layer was below the SIMS detection limit ($10^{16}/\text{cm}^3$), and no effect of In on $[V_{III}]$ was observed by PAS. There was no significant change in free carrier concentration with and without TMI flow, and the resistivity improvement was predominantly driven by mobility enhancement. TMI did not result in resistivity improvement at $T = 1175$ °C, perhaps because of higher desorption rates and reduced residence time of indium on the surface. However, further investigations are needed to fully understand how TMI flow during growth is impacting the AlGaIn:Si resistivity.

Low-resistivity higher Al content AlGaIn:Si was also developed using the optimal disilane/TMA ratio obtained from Fig. 2. For instance, we obtained 70% AlGaIn:Si grown at 950 °C with a resistivity of 10.5 mΩ cm and 83% AlGaIn:Si grown at 850 °C with a resistivity of 20 mΩ cm [Fig. 5(c)].²⁶ With further improvements in the AlN buffer layer,³⁴ we implemented this approach in developing high wall-plug efficiency UV LEDs.⁷⁸ Next, we implemented this approach in a different MOCVD reactor on a different SiC

polytype and achieved a further increase in the silicon concentration ($[\text{Si}] \sim 4 \times 10^{19}/\text{cm}^3$), which further decreased the resistivity of $\text{Al}_{0.65}\text{Ga}_{0.35}\text{N}:\text{Si}$ and $\text{Al}_{0.7}\text{Ga}_{0.3}\text{N}:\text{Si}$ to 4 and 6 $\text{m}\Omega\text{ cm}$, respectively, which is, to the best of our knowledge, the lowest resistivities reported for n -type $\text{Al}_x\text{Ga}_{1-x}\text{N}$ for $x > 0.6$,⁷⁹ including $\text{AlGaN}:\text{Si}$ films grown on native substrates,⁸⁰ which demonstrate the value of growing AlGaN over SiC .⁸¹

IV. CONCLUSION

In this work, we presented a method to realize highly conductive Al-rich $\text{AlGaN}:\text{Si}$ for photonic and electronic applications. The optimal Si doping window for the growth of low-resistivity Al-rich $\text{AlGaN}:\text{Si}$ was extended, and Si doping efficiency was increased by growing at lower growth temperatures and higher growth rates. Low-resistivity $\text{Al}_{0.65}\text{Ga}_{0.35}\text{N}:\text{Si}$ was processed using this method without compromising the surface morphology, impurity uptake, or cation monovacancies. PAS and SIMS experiments confirmed that $[\text{V}_{\text{III}}]$ and common impurity levels (H, C, O, and Mg) were insufficient to account for the apparent Si compensation behavior. TMI flow during $\text{AlGaN}:\text{Si}$ growth was found to reduce the resistivity by a factor of 2 without any measurable indium incorporation as confirmed by SIMS and no impact on $[\text{V}_{\text{III}}]$ as verified by PAS.

ACKNOWLEDGMENTS

This work was funded by the KACST-KAUST-UCSB Technology transfer program and the Solid State Lighting and Energy Electronics Center (SSLEEC) at UC Santa Barbara; a part of this work was carried out in the California NanoSystems Institute at UCSB. The research reported here made use of shared facilities of the UCSB MRSEC (Grant No. NSF DMR 1720256). A portion of this research was conducted in the UCSB nanofabrication facility, NSF NNIN network (Grant No. ECS-0335765). This work was partially funded by the Academy of Finland, Project No. 315082. The authors would like to gratefully thank Dr. Tom Mates for SIMS measurements and Dr. Stacia Keller and Dr. Mohammed Abo Alreesh for their insightful inputs. In addition, the authors would like to thank Dr. Youli Li from MRL and the cleanroom staff at the UCSB nanofabrication facility for the technical support provided.

DATA AVAILABILITY

The data that support the findings of this study are available from the corresponding author upon reasonable request.

REFERENCES

- R. J. Kaplar, A. A. Allerman, A. M. Armstrong, A. G. Baca, M. H. Crawford, J. R. Dickerson, E. A. Douglas, A. J. Fischer, B. A. Klein, and S. Reza, *Semiconductors and Semimetals* (Academic Press, Inc., 2019), pp. 397–416.
- A. M. Armstrong, B. A. Klein, A. Colon, A. A. Allerman, E. A. Douglas, A. G. Baca, T. R. Fortune, V. M. Abate, S. Bajaj, and S. Rajan, *Jpn. J. Appl. Phys., Part 1* **57**, 074103 (2018).
- J. Y. Tsao, S. Chowdhury, M. A. Hollis, D. Jena, N. M. Johnson, K. A. Jones, R. J. Kaplar, S. Rajan, C. G. Van de Walle, E. Bellotti, C. L. Chua, R. Collazo, M. E. Coltrin, J. A. Cooper, K. R. Evans, S. Graham, T. A. Grotjohn, E. R. Heller, M. Higashiwaki, M. S. Islam, P. W. Juodawlkis, M. A. Khan, A. D. Koehler, J. H. Leach, U. K. Mishra, R. J. Nemanich, R. C. N. Pilawa-Podgurski, J. B. Shealy,

- Z. Sitar, M. J. Tadjer, A. F. Witulski, M. Wraback, and J. A. Simmons, *Adv. Electron. Mater.* **4**, 1600501 (2018).
- R. J. Kaplar, A. A. Allerman, A. M. Armstrong, M. H. Crawford, J. R. Dickerson, A. J. Fischer, A. G. Baca, and E. A. Douglas, *ECS J. Solid State Sci. Technol.* **6**, Q3061 (2017).
- Y. Nagasawa, A. Hirano, Y. Nagasawa, and A. Hirano, *Appl. Sci.* **8**, 1264 (2018).
- N. Alfaraj, J.-W. Min, C. H. Kang, A. A. Alatawi, D. Priante, R. C. Subedi, M. Tangi, T. K. Ng, B. S. Ooi, N. Alfaraj, J.-W. Min, C. H. Kang, A. A. Alatawi, D. Priante, R. C. Subedi, M. Tangi, T. K. Ng, and B. S. Ooi, *J. Semicond.* **40**, 121801 (2019), Uncorrected proof.
- M. Kneissl, T.-Y. Seong, J. Han, and H. Amano, *Nat. Photonics* **13**, 233 (2019).
- Z. Zhang, M. Kushimoto, T. Sakai, N. Sugiyama, L. J. Schowalter, C. Sasaoka, and H. Amano, *Appl. Phys. Express* **12**, 124003 (2019).
- F. Roccaforte, G. Greco, P. Fiorenza, and F. Iucolano, *Materials* **12**, 1599 (2019).
- F. Mehnke, L. Sulmoni, M. Guttmann, T. Wernicke, and M. Kneissl, *Appl. Phys. Express* **12**, 012008 (2019).
- X. Liu, K. Mashooq, D. A. Laleyan, E. T. Reid, and Z. Mi, *Photonics Res.* **7**, B12 (2019).
- X. He, E. Xie, M. S. Islam, A. A. Purwita, J. J. D. McKendry, E. Gu, H. Haas, and M. D. Dawson, *Photonics Res.* **7**, B41 (2019).
- C. Xie, X.-T. Lu, X.-W. Tong, Z.-X. Zhang, F.-X. Liang, L. Liang, L.-B. Luo, and Y.-C. Wu, *Adv. Funct. Mater.* **29**, 1806006 (2019).
- J. Ruschel, J. Glaab, B. Beidoun, N. L. Ploch, J. Rass, T. Kolbe, A. Knauer, M. Weyers, S. Einfeldt, and M. Kneissl, *Photonics Res.* **7**, B36 (2019).
- M.-H. Chang, D. Das, P. V. Varde, and M. Pecht, *Microelectron. Reliab.* **52**, 762 (2012).
- W. W. Chow, M. Kneissl, J. E. Northrup, and N. M. Johnson, *Appl. Phys. Lett.* **90**, 101116 (2007).
- J. Li, K. B. Nam, J. Y. Lin, and H. X. Jiang, *Appl. Phys. Lett.* **79**, 3245 (2001).
- J. S. Harris, B. E. Gaddy, R. Collazo, Z. Sitar, and D. L. Irving, *Phys. Rev. Mater.* **3**, 054604 (2019).
- R. Blasco, A. Ajay, E. Robin, C. Bougerol, K. Lorentz, L. C. Alves, I. Mouton, L. Amichi, A. Grenier, and E. Monroy, *J. Phys. D: Appl. Phys.* **52**, 125101 (2019).
- L. Gordon, J. B. Varley, J. L. Lyons, A. Janotti, and C. G. Van de Walle, *Phys. Status Solidi RRL* **9**, 462 (2015).
- L. Gordon, J. L. Lyons, A. Janotti, and C. G. Van De Walle, *Phys. Rev. B* **89**, 085204 (2014).
- X. T. Trinh, D. Nilsson, I. G. Ivanov, E. Janzén, A. Kakanakova-Georgieva, and N. T. Son, *Appl. Phys. Lett.* **105**, 162106 (2014).
- N. T. Son, M. Bickermann, and E. Janzén, *Appl. Phys. Lett.* **98**, 092104 (2011).
- J. S. Harris, J. N. Baker, B. E. Gaddy, I. Bryan, Z. Bryan, K. J. Mirrieles, P. Reddy, R. Collazo, Z. Sitar, and D. L. Irving, *Appl. Phys. Lett.* **112**, 152101 (2018).
- Q. Yan, A. Janotti, M. Scheffler, and C. G. Van De Walle, *Appl. Phys. Lett.* **105**, 111104 (2014).
- F. Mehnke, T. Wernicke, H. Pingel, C. Kuhn, C. Reich, V. Kueller, A. Knauer, M. Lapeyrade, M. Weyers, and M. Kneissl, *Appl. Phys. Lett.* **103**, 212109 (2013).
- F. Mehnke, X. T. Trinh, H. Pingel, T. Wernicke, E. Janzén, N. T. Son, and M. Kneissl, *J. Appl. Phys.* **120**, 145702 (2016).
- P. Pampili and P. J. Parbrook, *Mater. Sci. Semicond. Process.* **62**, 180 (2017).
- Y. Shimahara, H. Miyake, K. Hiramatsu, F. Fukuyo, T. Okada, H. Takaoka, and H. Yoshida, *Jpn. J. Appl. Phys., Part 1* **50**, 095502 (2011).
- R. Collazo, S. Mita, J. Xie, A. Rice, J. Tweedie, R. Dalmau, and Z. Sitar, *Phys. Status Solidi* **8**, 2031 (2011).
- S. Hashimoto, K. Akita, T. Tanabe, H. Nakahata, K. Takeda, and H. Amano, *Phys. Status Solidi* **7**, 1938 (2010).
- B. Sarkar, S. Washiyama, M. H. Breckenridge, A. Klump, J. N. Baker, P. Reddy, J. Tweedie, S. Mita, R. Kirste, D. L. Irving, R. Collazo, and Z. Sitar, *ECS Transactions* (Electrochemical Society, Inc., 2018), pp. 25–30.
- S. Keller, P. Cantu, C. Moe, Y. Wu, S. Keller, U. K. Mishra, J. S. Speck, and S. P. Denbaars, *Jpn. J. Appl. Phys., Part 1* **44**, 7227 (2005).
- C. J. Zollner, A. Almogbel, Y. Yao, B. K. SaifAddin, F. Wu, M. Iza, S. P. DenBaars, J. S. Speck, and S. Nakamura, *Appl. Phys. Lett.* **115**, 161101 (2019).

- ³⁵B. K. SaifAddin, A. Almogbel, C. J. Zollner, H. Foronda, A. Alyamani, A. Albadri, M. Iza, S. Nakamura, S. P. DenBaars, and J. S. Speck, *Semicond. Sci. Technol.* **34**, 035007 (2019).
- ³⁶B. K. SaifAddin, M. Iza, H. Foronda, A. Almogbel, C. J. Zollner, F. Wu, A. Alyamani, A. Albadri, S. Nakamura, S. P. DenBaars, and J. S. Speck, *Opt. Express* **27**, A1074 (2019).
- ³⁷B. Saifaddin, C. J. Zollner, A. Almogbel, H. M. Foronda, F. Wu, A. Albadri, A. Al Yamani, M. Iza, S. Nakamura, S. P. DenBaars, and J. S. Speck, *Proc. SPIE* **10554**, 105541E (2018).
- ³⁸A. Almogbel, B. K. Saifaddin, C. Zollner, M. Iza, H. Albraithen, A. Alyamani, A. Albadri, S. P. DenBaars, S. Nakamura, and J. S. Speck, in 60th Electronic Materials Conference, Santa Barbara, CA, 2018.
- ³⁹H. M. Foronda, F. Wu, C. Zollner, M. E. Alif, B. Saifaddin, A. Almogbel, M. Iza, S. Nakamura, S. P. DenBaars, and J. S. Speck, *J. Cryst. Growth* **483**, 134 (2018).
- ⁴⁰B. K. SaifAddin, A. S. Almogbel, C. J. Zollner, F. Wu, B. Bonef, M. Iza, S. Nakamura, S. P. DenBaars, and J. S. Speck, *ACS Photonics* **7**, 554 (2020).
- ⁴¹F. Tuomisto and I. Makkonen, *Rev. Mod. Phys.* **85**, 1583 (2013).
- ⁴²R. Krause-Rehberg and H. S. Leipner, *Positron Annihilation in Semiconductors: Defect Studies* (Springer, 1999).
- ⁴³S. R. Lee, A. F. Wright, M. H. Crawford, G. A. Petersen, J. Han, and R. M. Biefeld, *Appl. Phys. Lett.* **74**, 3344 (1999).
- ⁴⁴P. Rinke, M. Winkelnkemper, A. Qteish, D. Bimberg, J. Neugebauer, and M. Scheffler, *Phys. Rev. B* **77**, 075202 (2008).
- ⁴⁵I. Vurgaftman and J. R. Meyer, *J. Appl. Phys.* **94**, 3675 (2003).
- ⁴⁶D. H. Reep and S. K. Ghandhi, *J. Electrochem. Soc.* **130**, 675 (1983).
- ⁴⁷D. D. Koleske, A. E. Wickenden, R. L. Henry, J. C. Culbertson, and M. E. Twigg, *J. Cryst. Growth* **223**, 466 (2001).
- ⁴⁸D. D. Koleske, A. E. Wickenden, R. L. Henry, and M. E. Twigg, *J. Cryst. Growth* **242**, 55 (2002).
- ⁴⁹S. Tanaka, M. Takeuchi, and Y. Aoyagi, *Jpn. J. Appl. Phys., Part 2* **39**, L831 (2000).
- ⁵⁰C. Stampfl and C. G. Van De Walle, *Appl. Phys. Lett.* **72**, 459 (1998).
- ⁵¹W. Walukiewicz, *Physica B* **302–303**, 123 (2001).
- ⁵²Y. Taniyasu, M. Kasu, and N. Kobayashi, *Appl. Phys. Lett.* **81**, 1255 (2002).
- ⁵³J. Oila, V. Ranki, J. Kivioja, K. Saarinen, P. Hautojärvi, J. Likonen, J. M. Baranowski, K. Pakula, T. Suski, M. Leszczynski, and I. Grzegory, *Phys. Rev. B* **63**, 045205 (2001).
- ⁵⁴J. M. Mäki, I. Makkonen, F. Tuomisto, A. Karjalainen, S. Suihkonen, J. Räisänen, T. Y. Chemekova, and Y. N. Makarov, *Phys. Rev. B* **84**, 081204 (2011).
- ⁵⁵F. Tuomisto, V. Prozhveeva, I. Makkonen, T. H. Myers, M. Bockowski, and H. Teisseyre, *Phys. Rev. Lett.* **119**, 196404 (2017).
- ⁵⁶A. Uedono, K. Tenjinbayashi, T. Tsutsui, Y. Shimahara, H. Miyake, K. Hiramatsu, N. Oshima, R. Suzuki, and S. Ishibashi, *J. Appl. Phys.* **111**, 013512 (2012).
- ⁵⁷S. F. Chichibu, A. Uedono, T. Onuma, T. Sota, B. A. Haskell, S. P. DenBaars, J. S. Speck, and S. Nakamura, *Appl. Phys. Lett.* **86**, 021914 (2005).
- ⁵⁸T. Onuma, S. F. Chichibu, A. Uedono, T. Sota, P. Cantu, T. M. Katona, J. F. Keadig, S. Keller, U. K. Mishra, S. Nakamura, and S. P. DenBaars, *J. Appl. Phys.* **95**, 2495 (2004).
- ⁵⁹J. Slotte, F. Tuomisto, K. Saarinen, C. G. Moe, S. Keller, and S. P. DenBaars, *Appl. Phys. Lett.* **90**, 151908 (2007).
- ⁶⁰S. F. Chichibu, H. Miyake, Y. Ishikawa, M. Tashiro, T. Ohtomo, K. Furusawa, K. Hazu, K. Hiramatsu, and A. Uedono, *J. Appl. Phys.* **113**, 213506 (2013).
- ⁶¹V. Prozhveeva, I. Makkonen, H. Li, S. Keller, U. K. Mishra, and F. Tuomisto, *Phys. Rev. Appl.* **13**, 044034 (2020).
- ⁶²I. Bryan, Z. Bryan, S. Washiyama, P. Reddy, B. Gaddy, B. Sarkar, M. H. Breckenridge, Q. Guo, M. Bodea, J. Tweedie, S. Mita, D. Irving, R. Collazo, and Z. Sitar, *Appl. Phys. Lett.* **112**, 062102 (2018).
- ⁶³A. Uedono, S. Ishibashi, N. Oshima, and R. Suzuki, *Jpn. J. Appl. Phys., Part 1* **52**, 08JJ02 (2013).
- ⁶⁴S. T. Bradley, S. H. Goss, L. J. Brillson, J. Hwang, and W. J. Schaff, *J. Vac. Sci. Technol. B* **21**, 2558 (2003).
- ⁶⁵S. Ishibashi, A. Uedono, H. Kino, T. Miyake, and K. Terakura, *J. Phys.: Condens. Matter* **31**, 475401 (2019).
- ⁶⁶J. L. Lyons and C. G. Van De Walle, *npj Comput. Mater.* **3**, 12 (2017).
- ⁶⁷P. C. Bowes, Y. Wu, J. N. Baker, J. S. Harris, and D. L. Irving, *Appl. Phys. Lett.* **115**, 052101 (2019).
- ⁶⁸Y. Gao, D. Sun, X. Jiang, and J. Zhao, *J. Appl. Phys.* **125**, 215705 (2019).
- ⁶⁹I. A. Aleksandrov and K. S. Zhuravlev, *J. Phys.: Condens. Matter* **32**, 435501 (2020).
- ⁷⁰C. G. Van De Walle and J. Neugebauer, *J. Appl. Phys.* **95**, 3851 (2004).
- ⁷¹T. Koppe, H. Hofsäss, and U. Vetter, *J. Lumin.* **178**, 267 (2016).
- ⁷²C. Wetzel, T. Suski, J. W. Ager, E. R. Weber, E. E. Haller, S. Fischer, B. K. Meyer, R. J. Molnar, and P. Perlin, *Phys. Rev. Lett.* **78**, 3923 (1997).
- ⁷³C. G. Van De Walle, *Phys. Rev. B* **57**, R2033 (1998).
- ⁷⁴C. Skierbiszewski, T. Suski, M. Leszczynski, M. Shin, M. Skowronski, M. D. Bremser, and R. F. Davis, *Appl. Phys. Lett.* **74**, 3833 (1999).
- ⁷⁵P. M. Mooney, T. N. Theis, and S. L. Wright, *Appl. Phys. Lett.* **53**, 2546 (1988).
- ⁷⁶T. M. Al Tahtamouni, A. Sedhain, J. Y. Lin, and H. X. Jiang, *Appl. Phys. Lett.* **92**, 092105 (2008).
- ⁷⁷E. C. H. Kyle, S. W. Kaun, E. C. Young, and J. S. Speck, *Appl. Phys. Lett.* **106**, 222103 (2015).
- ⁷⁸C. J. Zollner, A. S. Almogbel, Y. Yao, M. Wang, M. Iza, J. S. Speck, S. P. DenBaars, and S. Nakamura, *Opt. Mater. Express* **10**, 2171 (2020).
- ⁷⁹Y.-H. Liang and E. Towe, *Appl. Phys. Rev.* **5**, 011107 (2018).
- ⁸⁰S. Washiyama, P. Reddy, B. Sarkar, M. H. Breckenridge, Q. Guo, P. Bagheri, A. Klump, R. Kirste, J. Tweedie, S. Mita, Z. Sitar, and R. Collazo, *J. Appl. Phys.* **127**, 105702 (2020).
- ⁸¹C. Huang, H. Zhang, and H. Sun, *Nano Energy* **77**, 105149 (2020).